Numerical Analysis of Bird Strike on Engine Cowling of AW139 Helicopter using Sandwich Composite Material with Lattice Core Structure

Budi Aji Warsiyanto[1,*], Syarifah Fairuza[2], Muhammad Hadi Widanto[3], Gavin Mustika Kresna[4]

The Air Marshal Suryadarma Aerospace University, Jakarta, Indonesia[1,2,3,4]

budiajiwarsiyanto@gmail.com [1], fairuza@unsurya.ac.id[2] , mhadi@unsurya.ac.id[3], 181011003@students.unsurya.ac.id[3]

Abstract. Bird strikes can potentially damage the engine and body, disrupting flight safety. One of the helicopter components susceptible to bird strike is the engine cowling. This study aims to analyze the effect of sandwich structure core material variation on the impact response of the AW139 helicopter's engine cowling. The finite element method was used to analyze the strength of the engine cowling structure due to bird strike because it can effectively evaluate several structural designs. The bird model was modeled through Smooth Particle Hydrodynamics (SPH). This study uses sandwich composite material with foam, body-centered cubic (BCC) lattice, and foam-lattice hybrid cores. The lattice material was found to undergo buckling and plastic deformation at the impact area to absorb greater energy. The hybrid foam-lattice core material is stiffer, which reduces energy absorption and deformation. When the outer plate is thicker, the structure has better resistance to composite damage. Thinner outer plates provide better energy transfer to the core, leading to increased impact energy absorption, but can potentially cause premature breakage of the composite material.

Keywords: Bird strike, Engine cowling, SPH, Lattice structure, Sandwich Composite, AW139 Helicopter.

1 Introduction

Bird strike is a phenomenon of collisions between birds and vehicles, such as aircraft, which can potentially damage the engine and body, disrupting flight safety. One of the helicopter components that has the potential to be hit by a bird strike is the engine cowling. Certification Specification (CS) 29.631 states the rotorcraft must be designed to assure capability of continued safe flight and landing after impact with a 1 kg bird, when the velocity of the rotorcraft (relative to the bird along the flight path of the rotorcraft) is equal to V_{NE} or V_H (whichever is the lesser) at altitudes up to 2438 m (8 000 ft) [1].

Laminate composites are unable to achieve the desired properties and are often obtained through the combination of materials or sandwich structure [2]. In the impact

AVINER 2023, November 08-09, Jakarta, Indonesia

DOI 10.4108/eai.8-11-2023.2345975

phenomenon, the composite sandwich core has large compressive deformation and good energy absorption. The lattice structures provide high energy absorption and porosity [3]. Therefore, lattice materials have promising potential when used in aircraft structures [4].

Much research has been done on the resistance of sandwich and lattice structures. Yan et al. [5] studied the effect of foam on strength under compression loading. It was found that foam-filled plates have better strength and energy absorption capacity. Feng et al. [6] analyzed the hourglass and pyramid lattice structures. It was found that the hourglass lattice structure has better resistance than the pyramid lattice.

The resistance of sandwich structures with lattice core due to bird strikes is of great interest. Therefore, in this study, the numerical analysis of bird strike on the engine cowling of AgustaWestland AW139 helicopter using laminate composite material, sandwich composite with a foam core, sandwich composite with body-centered cubic (BCC) lattice core, and sandwich composite with hybrid foam-lattice core are conducted. In addition, the influence of sandwich structure configuration on the impact response is studied. The displacement and energy absorption of the curved plate, as well as composite damage, were also compared.

2 Methodology

2.1 Model Description

The AW139 helicopter engine cowling is modeled as a curved plate (see Fig. 1). The geometry of the plate was obtained from Giannaros et al. [7], where the length, width, thickness, and radius of the plate are shown in Fig. 2.

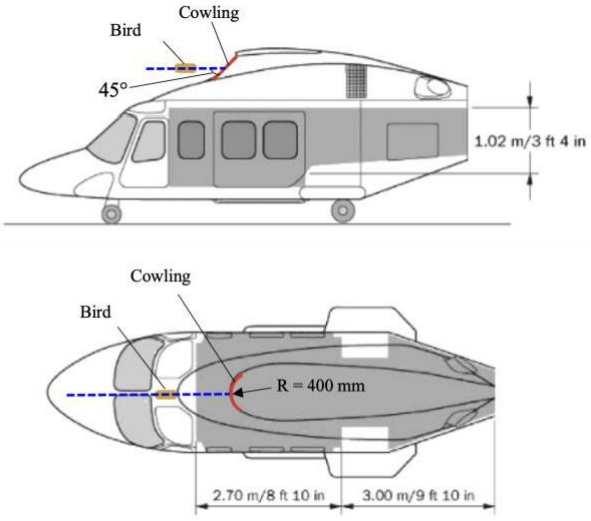

Fig. 1. Bird strike on AW139 helicopter scenario.

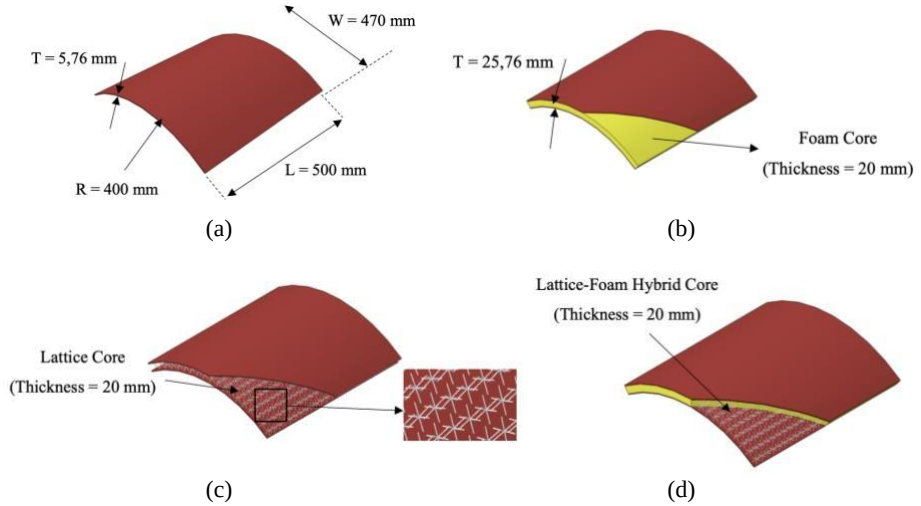

Fig. 2. Panel construction of AW139 helicopter: (a) laminate composite, sandwich with core, (b) foam, (c) lattice, (d) foam-lattice hybrid.

The lattice type used in this study is BCC, which has high strength and large stress distribution. The number of lattices in the sandwich structure is 475. Strut cross-sectional diameter (d), height (H), tilt angle (α), separation angle (β), and length (L) of lattice shown in Fig. 3.

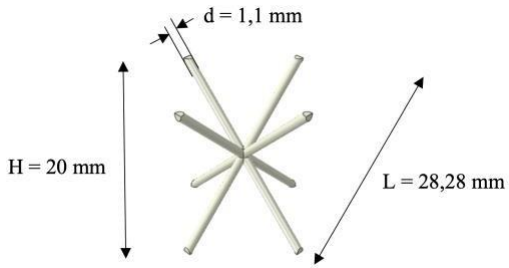

Fig. 3. Geometric and dimension of body-centered cubic unit cell lattice.

2.2 Numerical Modeling

Bird Material Modeling. The hemispherical-ended cylinder geometry used on the bird model (see Fig. 4(a)). The bird has a mass of 1 kg. The material properties of the bird are shown in Table 1. The method to model the behavior of bird material is smooth particle hydrodynamics (see Fig. 4(b)).

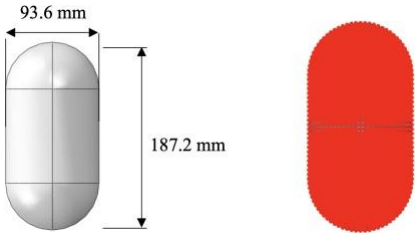

Fig. 4. Bird model: (a) geometry, (b) SPH

Table 1. Mechanical properties of bird material.

Density (kg/m^3)	Shear modulus (MPa)	Yield stress (MPa)
935	10	0.1

Bird Model Validation. Bird model validation was carried out by impact testing on a steel plate, which was compared with Wilbeck's experiment [8]. The plate has dimensions of 1000 x 1000 mm^2 with a thickness of 50 mm retained on its sides. The plate has 1540 shell elements (see Fig. 5). Mesh size of the bird model is 4 mm. The numerical simulation result shows good enough agreement with Wilbeck's experiment (see Fig. 6). Therefore, the bird model is valid to use in bird simulation on AW139's engine cowling.

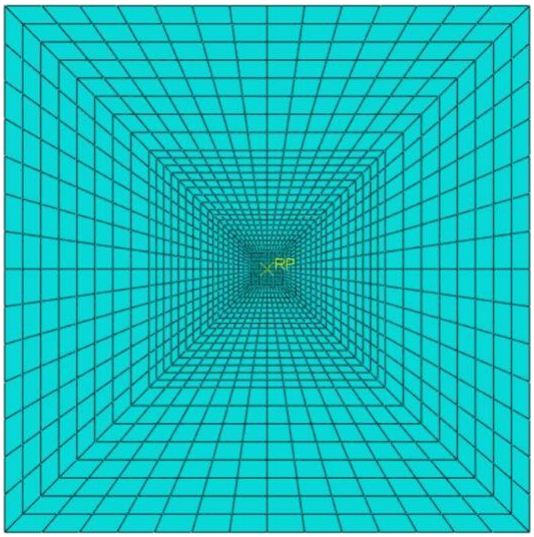

Fig. 5. Mesh of the plate

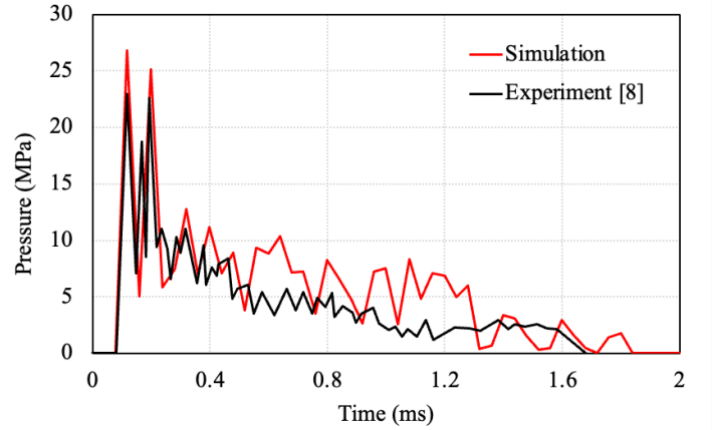

Fig. 6. Comparison of impact pressure between experimental testing and simulation

The material of composite plate is carbon fiber-epoxy resin with material properties as shown in Table 2. The thickness of the outer and inner plates of the composite sandwich structure is 5.76 mm, so the total thickness is 25.76 mm. The masses of the composite without core, foam core, lattice core, and foam-lattice hybrid core are 2.07 kg, 0.27 kg, 0.36 kg, 0.63 kg, respectively.

Table 2. Material properties of carbon-epoxy IM7/8552 [9].

Property	Value
E_1 (GPa)	165
E_2 (GPa)	9
E_3 (GPa)	9
ν_{12}	0.0185
ν_{13}	0.0185
ν_{23}	0.5
G_{12} (GPa)	5.6
G_{13} (GPa)	5.6
G_{23} (GPa)	2.8

This research predicts fiber tension, fiber compression, matrix tension, and matrix compression damage using the Hashin failure criterion [10]. The equation of failure criterion is written as follows:

Fiber tension, $(\sigma_{11} \geq 0)$:

$$\left(\frac{\sigma_{11}}{X^T}\right)^2 + \alpha\left(\frac{\tau_{12}}{S^L}\right)^2 = 1 \quad (1)$$

Fiber compression, $(\sigma_{11} < 0)$:

$$\left(\frac{\sigma_{11}}{X^C}\right)^2 = 1 \quad (2)$$

Matrix tension, $(\sigma_{22} \geq 0)$:

$$\left(\frac{\sigma_{22}}{Y^T}\right)^2 + \left(\frac{\tau_{12}}{S^L}\right)^2 = 1 \quad (3)$$

Matrix compression, $(\sigma_{22} < 0)$:

$$\left(\frac{\sigma_{22}}{2S^T}\right)^2 + \left[\left(\frac{Y^C}{2S^T}\right)^2 - 1\right]\frac{\sigma_{22}}{Y^C} + \left(\frac{\tau_{12}}{S^L}\right)^2 = 1 \quad (4)$$

Mesh Convergence of Curved Plate. Composite laminate plate verification is conducted using the convergence of mesh. The meshing size was varied from 8 mm to 3 mm. As shown in Fig. 7, the mesh size is converged at 4 mm. A mesh size of 4 mm is equivalent to a number of 15876 elements.

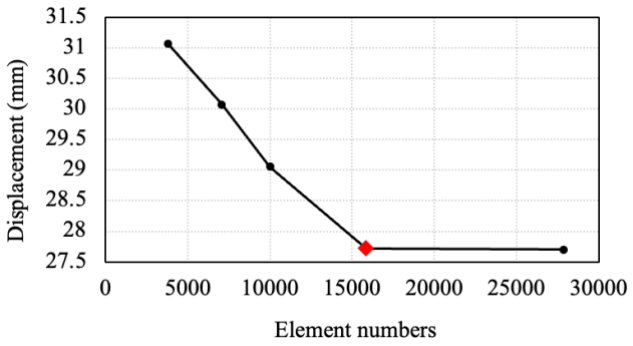

Fig. 7. Mesh convergence study result of composite curved plate.

Polyurethane Foam Material Model. The polyurethane (PU) foam is modelled using solid elements and its material properties are shown in Table 3. The mesh size for the foam model is 4 mm to avoid the hourglass phenomenon during impact. A comparison of simulation and experimental results is shown in Fig. 8. The model used shows the fit with the experimental result.

Table 3. Mechanical properties of PU foam material [11].

Density (kg/m^3)	Young's modulus (MPa)	Poisson's ratio
60	7.17	0.3

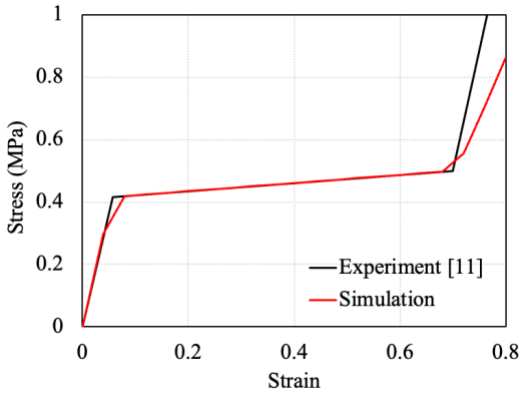

Fig. 8. PU foam material stress-strain curve [11].

Lattice Material Model. The BCC lattice is made from AISI material 304 stainless steel and simulated with an elastic-plastic material model. The material properties of 304 stainless steel are shown in Table 4. The stress-strain curve of 304 stainless steel is shown in Fig. 9. Each unit uses 32 beam elements with an element size of 3.5 mm.

The thickness of the outer and inner plates is maintained at 5.76 mm. The panel configuration of the sandwich structure's effect on the resistance of the panel was studied by using different thicknesses for the outer and inner plates. Tables 5 and 6 show the configuration of panel and panel lay-ups, respectively.

Table 4. Mechanical properties of 304 stainless steel material [12].

Density (kg/m^3)	Young's modulus (GPa)	Poisson's ratio	Yield stress (MPa)
7900	193	0.3	550

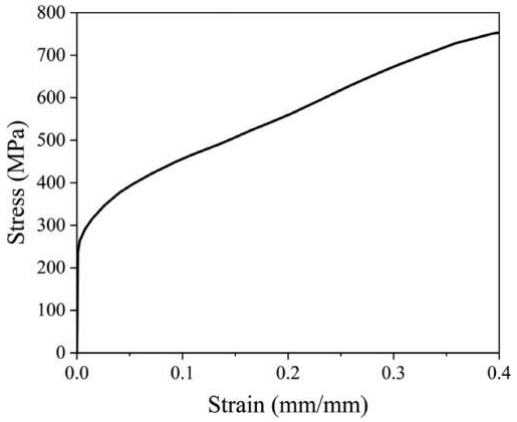

Fig. 9. The 304 stainless steel stress-strain curve [12].

Table 5. Thickness distribution of the outer and inner plate.

Panel configurations	Outer plate	Inner plate
P1	2.88 mm	2.88 mm
P2	1.44 mm	4.32 mm
P3	4.32 mm	1.44 mm

Table 6. Ply angles of the outer and inner plate.

Panel configurations	Outer plate	Inner plate
P1	$(45/0/-45/90/90/-45/0/45)_s$	$(45/0/-45/90/90/-45/0/45)_s$
P2	$(45/0/-45/90)_s$	$(45/0/-45/90/90/-45/0/45/45/0/-45/90)_s$
P3	$(45/0/-45/90/90/-45/0/45/45/0/-45/90)_s$	$(45/0/-45/90)_s$

Finite Element Model of Sandwich Structures. The velocity used in this simulation is 86 m/s, which is considered based on CS 29.631. Boundary conditions are applied at the edge of the cowling segment, as shown in Fig. 10. The boundary conditions used are of the fixed type that restrain translational and rotational motion about the X, Y, and Z axes.

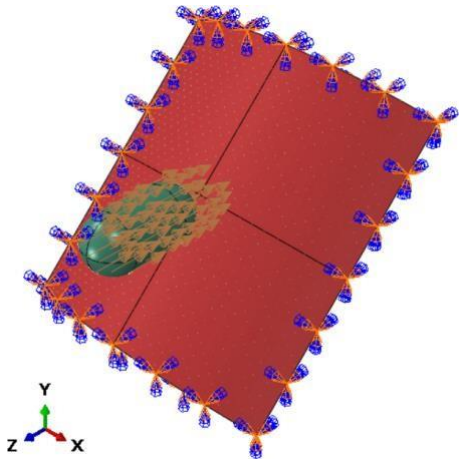

Fig. 10. Velocity and boundary condition of bird strike simulation.

3. Results and Discussion

3.1 Core Material Variation

Fig. 11 shows the deformation of panels with variations in core material has a similar trend. The lowest deformation occurs in the foam-lattice hybrid material of 25.49 mm, which describe the best resistance compared to the other two cores. The largest displacement occurred in the panel with a foam core of 31.22 mm.

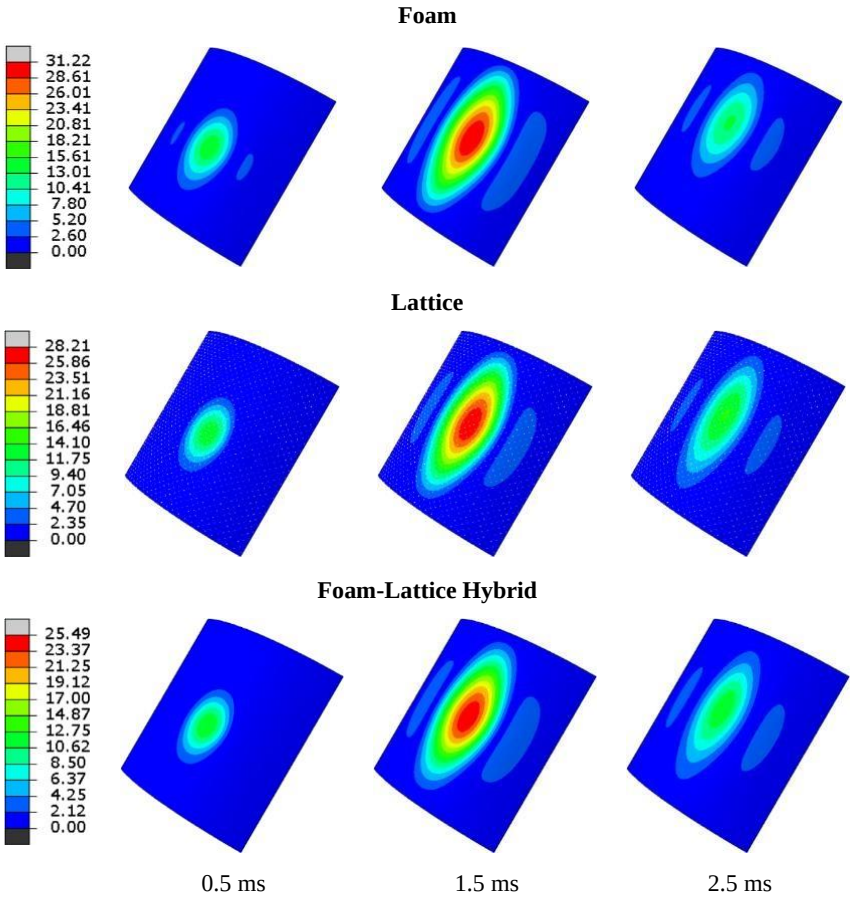

Fig. 11. Deformation of sandwich panel with core material variation.

Fig. 12 shows the displacement history of the outer and inner plates for different core materials. Displacements of the outer and inner plates for the foam core material are the largest compared to the other two materials because the stiffness of the foam material is the lowest.

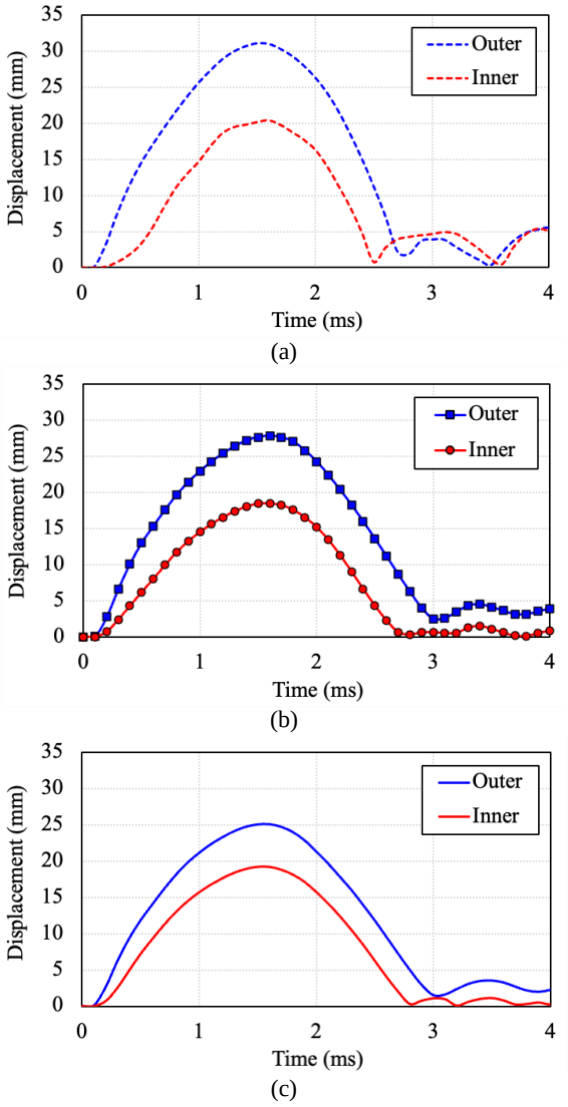

Fig. 12. Displacement of the outer and inner plates for different core materials: (a) foam, (b) lattice, and (c) foam-lattice hybrid.

The maximum displacement in the sandwich structure with the foam core material is 20.44 mm. The decrease in inner plate displacement from foam to lattice material is 6.4%, while the decrease in inner plate displacement from lattice to foam-lattice hybrid material is 4.1%.

The energy absorbed by the sandwich structure for different core materials is shown in Fig. 13. The sandwich structure with lattice core material has the highest energy absorption, as it absorbs energy through buckling and plastic deformation mechanisms.

The maximum energy absorption of the sandwich structure with foam, lattice, and foam-lattice hybrid cores are 1.05; 1.02; and 0.95 kJ, respectively. The foam-lattice hybrid material has the highest stiffness, making the panel stiffer than the other core materials.

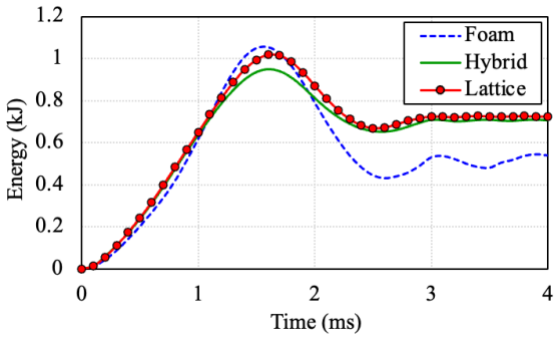

Fig. 13. Energy absorption of sandwich structure for different core materials.

The matrix damage in the outer plate for different core materials is shown in Fig. 14. In all core materials, matrix damage occurs in the plate. Similar to the matrix damage in the outer plate, the matrix and fiber damage in the inner plate is also concentrated in the center of the impact location (see Fig. 15 and Fig. 16). Unlike the outer plate, matrix and fiber damage in the inner plate does not occur because the core material mostly absorbs the impact energy through deformation.

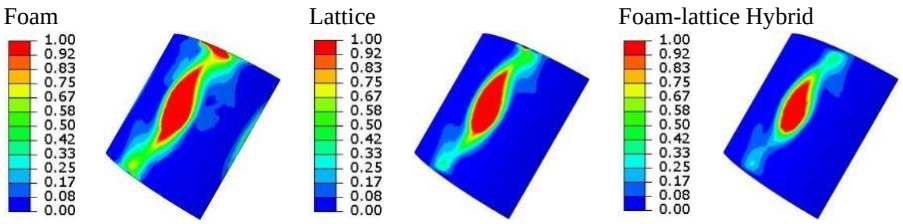

Fig. 14. Matrix damage in the outer plate for different core materials.

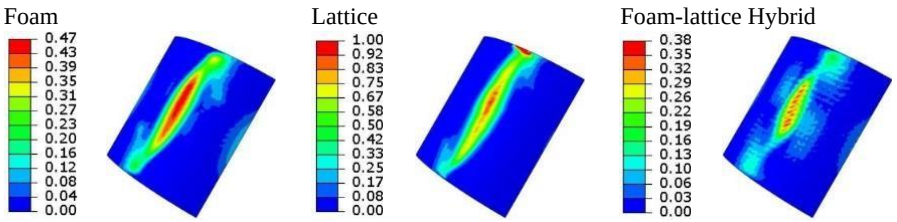

Fig**. 15.** Matrix damage in the inner plate for different core materials.

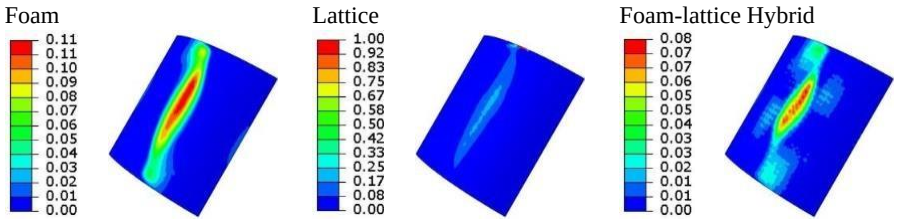

Fig. 16. Matrix damage in the inner plate for different core materials.

3.2 Thickness Variation of Outer and Inner Plates

In this section, the analysis was carried out on the outer and inner plate thickness variation. The effect of outer and inner plate thickness on panel response due to bird strike is studied using an impact angle of 45° and lattice core material.

Fig. 17 shows the deformation of the panel with varying thicknesses of the outer and inner plates. Overall, the deformation trend for panels with different plate thickness tends to be the same. The maximum deformation occurs in the middle of the simulation, at a time of 1.5 ms. The lowest deformation, 23.31 mm, occurs in the configuration of P3, which means the thickness of the outer plate is greater. In the P3 configuration, the stiffness of the outer plate increases. The highest deformation, 39.22 mm, occurs in the configuration of P2, which means the thickness of the outer plate is thinner.

Fig.18 shows the displacement history of the outer and inner plates for the thickness variation. The displacement of the inner plate is smaller than the outer plate due to the cushioning effect of the core material. It is found that the difference in plate thickness affects the deformation of the panel. The highest maximum displacement of the inner plate occurred in panel configuration P2 (thinner outer plate) at 26.19 mm. The difference in displacement of the panels in P3 and P2 configurations was 43.27% (similar to P1 and P2).

The energy absorbed by the panel for different thickness configurations P1, P2, and P3 is shown in Fig. 19. Configuration P2 has the greatest energy absorption, as the thinner outer plate allows greater transfer of energy from the birds to the core material. The lattice deformation indicates energy absorption through buckling and plastic deformation mechanisms. The maximum energy absorption of the sandwich panels with configurations P1, P2, and P3 are 1.02; 1.3; and 0.83 kJ, respectively. Configuration P3 has the lowest energy absorption because the thicker outer plate results in higher stiffness, so the energy transferred and absorbed by the lattice becomes smaller. The internal energy shown in Fig. 19 is the energy due to elastic and plastic deformation.

The matrix damage on the outer plate for different thickness configurations is shown in Fig. 20. In all thickness configurations, matrix damage occurred on the plate. The most extensive damage occurred in the P2 thickness configuration because the thinner thickness of the outer plate makes the stiffness lower and insufficient to withstand the impact load.

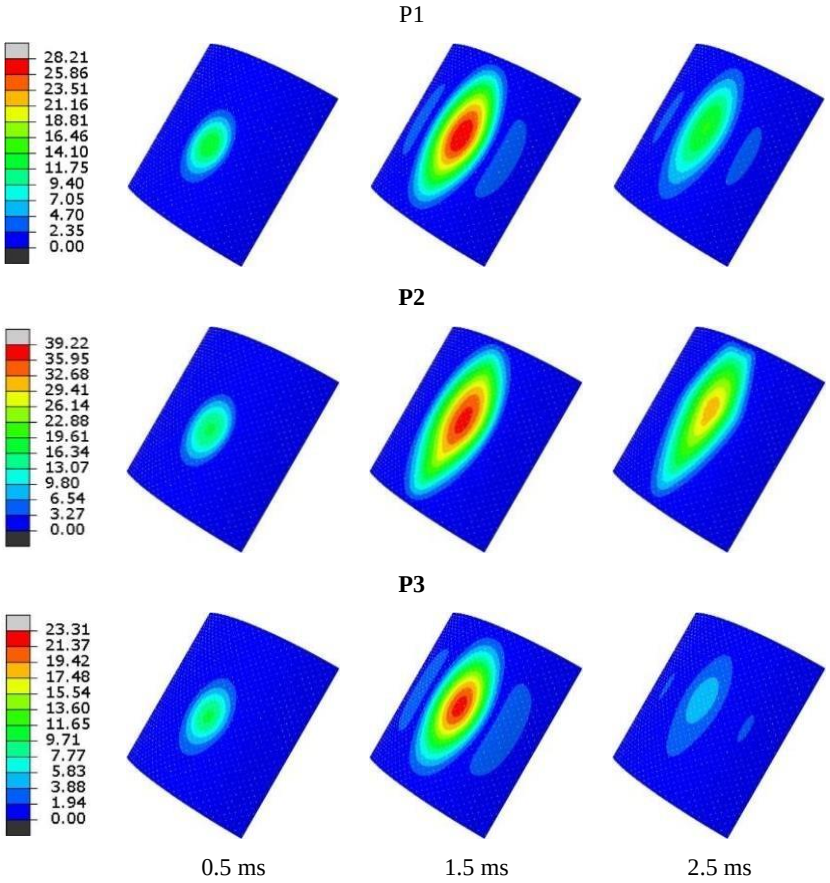

Fig. 17. Deformation of sandwich panel with core material variation.

The matrix and fiber damage in the inner plate is also concentrated at the center of the impact location (see Fig. 21 and Fig. 22). The damage spreads along the longitudinal direction of the plate. Configuration P2 shows damage in the matrix and fibers of the inner plate. The panel thickness configuration can affect the deformation and energy absorption. When the outer plate is thicker, the structure has more resistance to damage composites caused by bird strikes. The thinner outer plate provides better energy transfer to the core material, leading to an increased absorption impact energy.

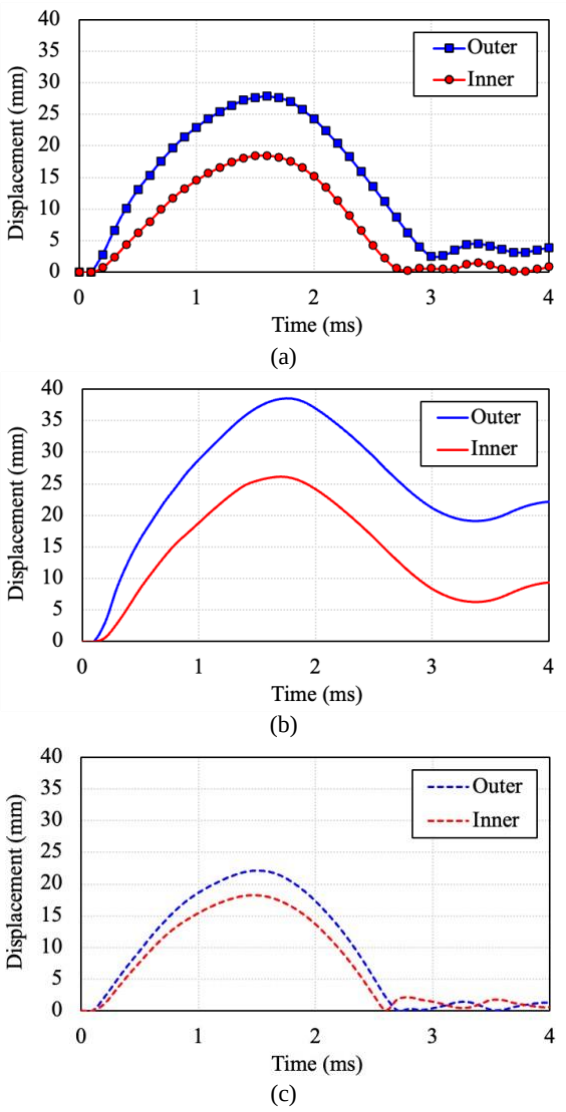

Fig. 18. Displacement of the outer and inner plates for different thicknesses of outer and inner plates: (a) P1, (b) P2, and (c) P3.

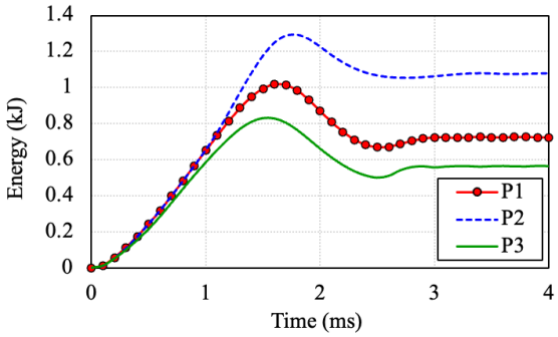

Fig. 19. Energy absorption of sandwich structure for different outer and inner plate thicknesses.

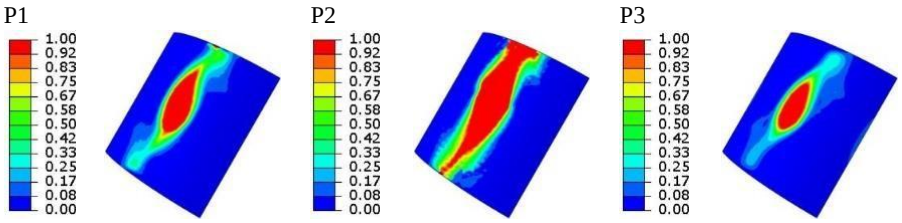

Fig. 20. Matrix damage in the outer plate for different thicknesses of the outer and inner plate.

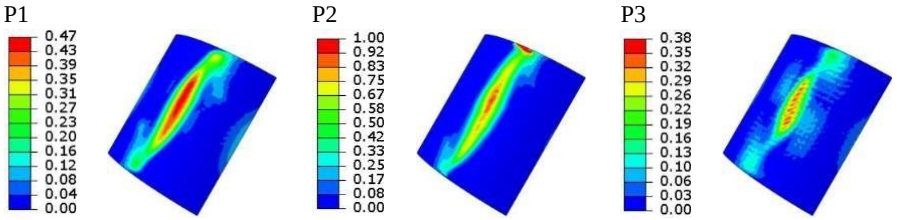

Fig. 21. Matrix damage in the inner plate for different thicknesses of the outer and inner plate.

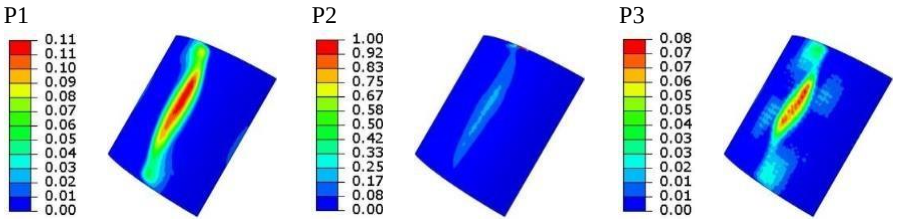

Fig. 22. Matrix damage in the inner plate for different thicknesses of the outer and inner plate.

4. Conclusion

Based on the analysis conducted on the parameters of deformation behavior, energy absorption, and damage of the composite, it was found that the core material can affect the deformation and energy absorption of the panel. The panel with foam core material has the largest deformation compared to the other two core materials. This indicates the foam material has the lowest impact resistance. The lattice material undergoes plastic deformation and buckling at the impact area to absorb more energy so that the energy transferred to the inner plate becomes smaller. The hybrid foam-lattice core material is stiffer, which reduces energy absorption and deformation. In terms of composite damage, all core materials have been unable to prevent damage to the outer plate due to bird strikes.

Panel thickness configuration can significantly affect deformation and energy absorption. When the outer plate is thicker, the panel has better resistance to composite damage caused by bird strikes. Thinner outer plates provide better energy transfer to the core material, leading to increased impact energy absorption. However, thinner outer plates can potentially cause premature damage of the composite material. The largest deformation and energy absorption occurred in the P2 configuration.

For further research, it is expected to be able to add simulation parameters, such as bird speed and bird mass. In addition, modeling mesoscale damage to composites, such as delamination, requires solid elements for the outer and inner plates.

References

1. European Union Aviation Safety Agency: Certification Specifications, Acceptable Means of Compliance and Guidance Material for Large Rotorcraft Amendment 9 (2021).
2. Georgiadis, S., Gunnion, A.J., Thomson, R.S., Cartwright, B.K.: Bird-strike simulation for certification of the Boeing 787 composite moveable trailing edge, Composites Structure, vol. 86, pp. 258–268 (2008).
3. Ozdemir, Z., Hernandez-Nava, E., Tyas, A., Warren, J.A., Fay, S.D., Goodall, R., Todd, I., Askes, H.: Energy absorption in lattice structures in dynamics: Experiments, International Journal of Impact Engineering, vol. 89, pp. 49–61 (2016).
4. Moongkhamklang, P., Elzey, D.M., Wadley, H.N.G.: Titanium matrix composite lattice structures, Composites, vol.39, pp. 176–187 (2008).
5. Yan, L.L., Yu, B., Han, B., Chen, C.Q., Zhang, Q.C., Lu, T.J.: Compressive strength and energy absorption of sandwich panels with aluminum foam-filled corrugated cores, Composites Science and Technology, vol. 86, pp. 142–148 (2013).
6. Feng, L.J., Wei, G.T., Yu, G.C., Wu, L.Z.: Underwater blast behaviours of enhanced lattice truss sandwich panels, International Journal of Mechanical Science, vol.150, pp. 238–246 (2019).
7. Giannaros, E., Kotzakolios, A., Kostopoulos, V., Sotiriadis, G., Vignjevic, R., Djordjevic, N., Boccaccio, M., Meo, M.: Low- and high- fidelity modeling of sandwich-structured composite response to Bird strike, as tools for a digital-twin-assisted damage diagnosis, International Journal of Impact Engineering, vol.160, 104058 (2022).
8. Wilbeck, J. S.: Impact Behavior of Low Strength Projectiles, Technical Reports AFML-TR-77-134, Air Force Materials Laboratory, Air Force Wright Aeronautical Laboratories, Air Force Systems Command, Wright-Patterson Air Force Base, Ohio (1978).

9. Cherniaev, A., Montesano, J., Butcher, C.: Modeling the axial crash response of CFRP tubes using MAT 054, MAT058 and MAT262 in LS-DYNA, in:15th LS-DYNA Users Conf Compos, pp. 1-17 (2018).
10. Hashin, Z.: Failure Criteria for Unidirectional Fiber Composites, Journal of Applied Mechanics, vol. 47, pp. 329–334 (1980).
11. Chen, J., Fang, H., Liu, W., Zhu, L., Zhuang, Y., Wang, J., Han, J.: Energy absorption of foam-filled multi-cell composite panels under quasi-static compression, Composites B, vol. 153, pp. 295-305 (2018).
12. Fan, W., Shen, D., Zhang, Z., Huang, X., Shao, X.: A Novel UHPFRC-based protective structure for bridge columns against vehicle collision: Experiment, simulation, and optimization, Eng. Struct., Vol. 207, 110247 (2020).